Robotics and Autonomous Systems 57 (2009) 1028–1035

Contents lists available at ScienceDirect

Robotics and Autonomous Systems

journal homepage: www.elsevier.com/locate/robot

Global indoor self-localization based on the ambient magnetic field

Janne Haverinen *, Anssi Kemppainen

University of Oulu, Department of Electrical and Information Engineering, Computer Engineering Laboratory, Erkki Koiso-Kanttilan katu 3, FIN-90014 University of Oulu, Finland

ARTICLE INFO

Article history:
Available online 26 July 2009

Keywords:
Monte Carlo localization
Mobile robot
Magnetic field

ABSTRACT

There is evidence that animals utilize local anomalities of Earth's magnetic field not just for orientation detection but also for true navigation, *i.e.*, some animals are not only able to detect the direction of Earth's magnetic field (compass heading), they are able to derive positional information from local cues arising from the local anomalities of Earth's magnetic field. Similarly to Earth's non-constant magnetic field, the magnetic field inside buildings can be highly non-uniform. The magnetic field fluctuations inside buildings arise from both natural and man-made sources, such as steel and reinforced concrete structures, electric power systems, electric and electronic appliances, and industrial devices. Assuming that the anomalities of the magnetic field inside a building are nearly static and they have sufficient local variability, the anomalies provide a unique magnetic fingerprint that can be utilized in global self-localization. Based on the evidence presented in this article it can be argued that this hypothesis is valid. In this article, a Monte Carlo Localization (MCL) technique based on the above hypothesis is proposed. The feasibility of the technique is demonstrated by presenting a series of global self-localization experiments conducted in four arbitrarily selected buildings, including a hospital. The experiment setup consists of a mobile robot instrumented with a 3-axis magnetometer and a computer. In addition to global robot self-localization experiments, successful person self-localization experiments were also conducted by using a wireless, wearable magnetometer. The reported experiments suggest that the ambient magnetic field may remain sufficiently stable for longer periods of time giving support for self-localization techniques utilizing the local deviations of the magnetic field.

1. Introduction

Evidence suggests that animals utilize Earth's magnetic field for navigation [1–5] and for orientation detection [6]. Some animals, such as spiny lobsters, are not only able to detect the direction of Earth's magnetic field, they can even sense their true position relative to their destination [1]. This means that these particular animals are able to derive positional information from local cues that arise from the local anomalies of Earth's magnetic field. The exact degree of magnetic sensitivity of lobsters is not known. However, the theoretical considerations seem to suggest that biological receptors can achieve the sensitivity required to use magnetic maps over distances as small as 10 km [7]. It has been argued that magnetic field sensitivity in living organisms is the result of a highly evolved, finely-tuned sensory system based on single domain, ferromagnetic crystals [8]. In [8], the authors also suggest that magneto reception could have been one of the first sensory systems that has been evolved. In this article, we propose an approach for global self-localization, which draws its inspiration from the nature and this intriguing ability of some animals to utilize the small deviations of Earth's magnetic field for true navigation. As an analog to the non-uniform magnetic field of the Earth, many buildings seems to have their own, distinguishable magnetic field with small local anomalities, as is illustrated in Fig. 10. By utilizing probabilistic techniques, such as MCL [9,10], these magnetic fields can provide a medium for indoor navigation.

Static and extremely low-frequency (ELF) magnetic fields in modern buildings arise from both natural and man-made sources, such as electric power systems, electric and electronic appliances, and industrial devices [11,12]. Steel and reinforced concrete structures of buildings cause fluctuations in the ambient magnetic field [13,14]. Static and ELF fields are mainly considered to be harmful, as they can cause electromagnetic interferences to sensitive electrical devices such as video display units and sophisticated measurement instruments. The health impacts of magnetic fields on people have also been studied [12], and solutions for eliminating the interference problems that magnetic fields cause in electronic devices and for alleviating concerns about possible health impacts have been proposed [11].

In this article the local anomalities of the ambient magnetic field are utilized in global indoor self-localization. It is argued here that each building has its own unique ambient magnetic field. If the anomalies of the magnetic field have sufficient variability, it is possible to utilize the field in the problem domain of mobile robot localization.

* Corresponding author. Tel.: +358 505172355.
E-mail address: janne.haverinen@ee.oulu.fi (J. Haverinen).

0921-8890/$ – see front matter © 2009 Elsevier B.V. All rights reserved.
doi:10.1016/j.robot.2009.07.018

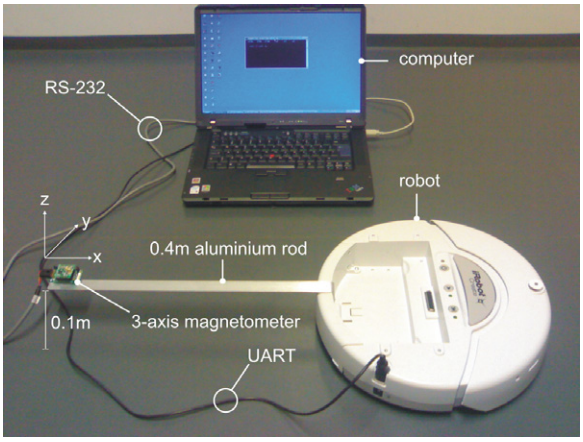

Fig. 1. The measurement setup used in global robot self-localization experiments. Sensor readings are transmitted to PC for storing through RS-232 connection.

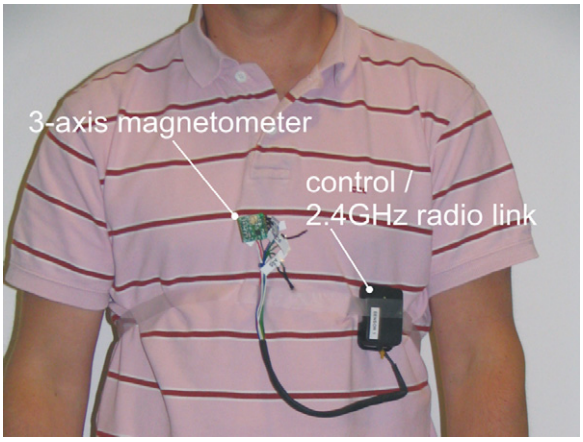

Fig. 2. The measurement setup used in global person self-localization experiments. 2.4 GHz radio link is used to send sensor readings to a base station, which stores the data.

Earth's magnetic field has been extensively utilized in detecting the heading of a robot by using an electric compass. Approaches to overcome the problems caused by magnetic field fluctuations to systems based on the electric compass have also been proposed [15]. Consequently, magnetic anomalities have been considered as an undesired property of the environment, when it comes to navigation. Only one previous study [16] was found where the ambient magnetic field has been utilized for localization. The authors of [16] used deviations of compass headings to provide distinctive location signatures for place recognition. However, in this article the local properties of the magnetic field are used as observations providing a spatially changing physical quantity, assuming a non-uniform magnetic field. In this article, MCL technique [9,10] was used to estimate the position of the robot, knowing the observations of the magnetic field and the approximate dynamics of the robot or a moving target (e.g. a person) in general. In this article, global self-localization was considered in one dimension only, *i.e.*, only the position of the target within the corridors was estimated. One-dimensional localization alone is useful in many applications, such as in office delivery applications. This is especially true in buildings where long corridors have been used to connect various parts, such as rooms, of the building.

The proposed approach is analogous to terrain navigation techniques, which have been used, *e.g.*, in autonomous underwater vehicles (AUV) [17–19]. The authors of [18] have proposed a concept of a magnetic terrain navigation system for submersibles, which utilizes the non-uniformity of Earth's magnetic field for underwater navigation.

This article is organized as follows. The experimental setup is described in Section 2.1. Section 2.2 briefly outlines the MCL technique. In Section 3 the calibration of the measurement system for compensating possible sensor inclination errors is briefly addressed. Section 4 presents the achieved results and the conclusion is given in Section 5.

2. Experiments

2.1. Setup

The framework of all buildings, used as experiment environments, are been made from reinforced concrete and steel. A floor plan example of one experiment environment is shown in Fig. 3, which presents the Computer Engineering laboratory (CL). Photos of interiors of all four experiment environments are shown in Fig. 4. The floor plan of Computer Engineering Laboratory shows the 278 m long measurement path through the main corridors of the laboratory. The path is marked with arrows in Fig. 3, starting from the 0 position and ending at the 278 position. The goal of each global self-localization experiment was to estimate the position of the localization target along the path through the environment while the robot or person was following approximately the centerline of the corridor. In each experiment the target (robot or person) started from an unknown initial position between $[0, x_{\max}]$. The fact that the localized target was following the centerline of the corridor made the localization problem one dimensional, *i.e.*, only the position of the localization target along the path was estimated. The measurement setup for global robot self-localization experiments is presented in Fig. 1. The robot used was iRobot's Create mobile robot, which was instrumented with a PNI MicroMag 3-axis magnetometer mounted at the end of a 0.4 m long aluminum rod in order to keep the magnetometer away from the magnetic field produced by the coils of the wheel motors. The magnetic field $\boldsymbol{B}$ was measured every 200 ms (5 Hz) producing a three-dimensional vector $\boldsymbol{m} = [m_x m_y m_z]$ consisting of the three components, in units of μT, of the magnetic flux density in x, y, and z directions, respectively (see Fig. 1).

Two alternative ways of utilizing the measurement $\boldsymbol{m}$ as an observation for the localization method were considered here: (1) using the norm $\|\boldsymbol{m}\|$ as the observation z from $\boldsymbol{B}$, and (2) using $\boldsymbol{m}$ directly as the observation $\boldsymbol{z}$. $\|\boldsymbol{m}\|$ is a rotation invariant scalar quantity assuming the magnetic sensor has been properly calibrated, *i.e.*, $\|\boldsymbol{m}\|$ provides information only about the magnitude of the magnetic field. The use of $\|\boldsymbol{m}\|$ as the observation is justified when the angular motion of the sensor cannot be estimated nor controlled but the linear motion of the sensor can be estimated. When both linear and angular motion of the sensor can be estimated the best localization performance can be achieved by using $\boldsymbol{m}$ directly as the observation from the magnetic vector field $\boldsymbol{B}$.

The measurement setup for person self-localization experiments is presented in Fig. 2. The 3-axis magnetometer was located on person's chest from which the data is being sent to the control unit, which sends the data wirelessly to a base station for storing. Magnetic maps of paths through the experiment environments were provided prior to the localization experiments. Each map used in robot self-localization experiments was created by driving the robot under manual control along the path while keeping the robot approximately at the centerline of the corridor. The speed of the robot was 0.2 m/s and the magnetic field was measured at 5 Hz together with the position estimate, *i.e.*, the distance traveled by the robot from the origin (see Fig. 3). The final map was created by

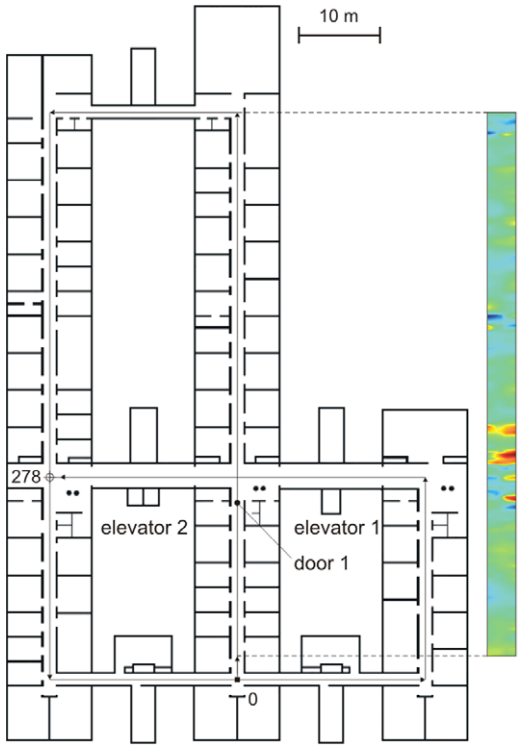

Fig. 3. Floor map of Computer Engineering Laboratory. The 0 position (label 0) and the end position (label 278) are marked with a square and a circle, respectively. The measurement path through the corridor is shown with arrows. The goal of global self-localization experiments is to estimate the position of the localization target (robot or person) that starts from an unknown position x_{start} between [0 m, 278 m] and goes along the path to selected, arbitrary direction. Two-dimensional map (see Fig. 10) for the first 70 m of the path is shown on the right.

applying a linear interpolation to data using a 0.04 m step size. The magnetic maps for the four experiment environments are shown in Fig. 5 showing $\|\boldsymbol{m}\|$ as a function of the position together with observation data which were acquired after the map data. In all experiments, map data was used as the ground truth, *i.e.*, possible odometric errors were not considered even though the errors introduce position deviations with respect to the real environment. In this article only the basic localization technique is considered — issues considering the accuracy of the map are not addressed here.

In person self-localization experiments odometric data (control) was not available. The preliminary global person localization experiments were conducted by taking magnetic field measurements while the person was walking approximately with constant speed (roughly 0.5 m/s). Deviations in walking speed caused some bias to the estimation error due to discrepancies between map and observation data. Despite this, the localization estimate converged near the true position. The future work will address the issue of estimating person's dynamics by utilizing inertial sensors in order to estimate the control applied to person's state.

In addition to the map data, observation data sets were acquired and used as observation (measurement) data in the reported experiments. After acquiring the observation data sets, the localization experiments were conducted off-line in Matlab environment using a simulated localization target, *i.e.*, a robot or a person. The localization target is using the collected observation data, *i.e.*, the function $h_{obs}(\boldsymbol{x})$, to generate an observation $\boldsymbol{z}$ for state $\boldsymbol{x}$. The observation data ($\|\boldsymbol{m}\|$ as a function of position x) are presented in Fig. 5 together with the map data. The legends in Fig. 5 show when the corresponding observation data was acquired, *i.e.*, t defines how many *days* have elapsed from the creation of the map.

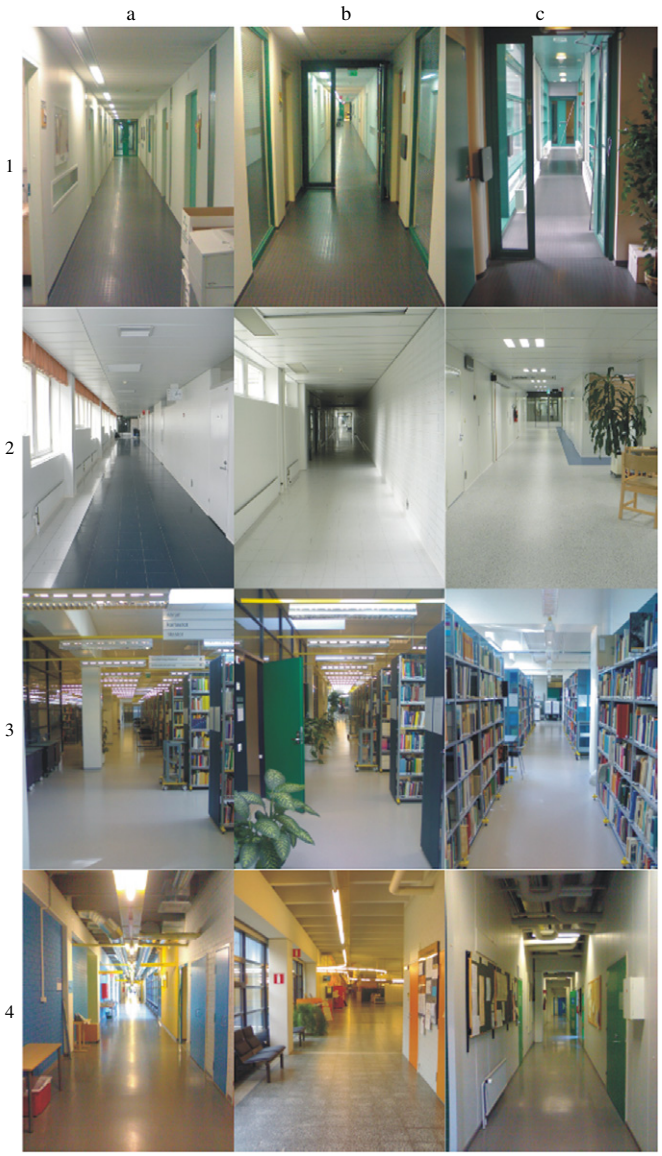

Fig. 4. Photos of the interiors of buildings where localization experiments were conducted (rows 1–4, path lengths in parentheses): (1) Computer Engineering Laboratory (278 m); (2) University hospital of Oulu (138 m); (3) a campus library of University of Oulu (93 m); and (4) Campus of University of Oulu (367 m). All the measurements were performed in the daytime during arbitrary office hours. The environments were not prepared in anyway for the measurements, except for opening the doors of the corridors in advance, which had some effects on the measurements.

2.2. Method

MCL [9,10] was utilized in order to estimate the position of the localization target starting from an unknown position x_{start} and following the centerline of the corridor thereafter. MCL utilizes a particle filter method [20,21,9,10] to approximate the distribution $p(x_t|z_t)$ when it is too complicated to sample directly, but when prior $p(x_t)$ can be sampled and the measurement density $p(z_t|x_t)$ can be evaluated. The particle filter utilizes importance sampling, which proceeds by generating a set of N samples $s^{(n)}$ from *a priori* $p(x_t)$ and then assigning to each sample a weight $\pi^{(n)} = p(z_t|x = s^{(n)})$ corresponding to the measurement density. The $\pi^{(n)}$ are normalized to sum 1 and then the weighted set $\{(s^{(n)}, \pi^{(n)})\}$ represents an approximation $\tilde{p}(x_t|z_t)$ of the desired *posterior* $p(x_t|z_t)$, where a sample is drawn from $\tilde{p}(x_t|z_t)$ by choosing one of the $s^{(n)}$ with probability $\pi^{(n)}$. As $N \to \infty$ samples from $\tilde{p}(x_t|z_t)$

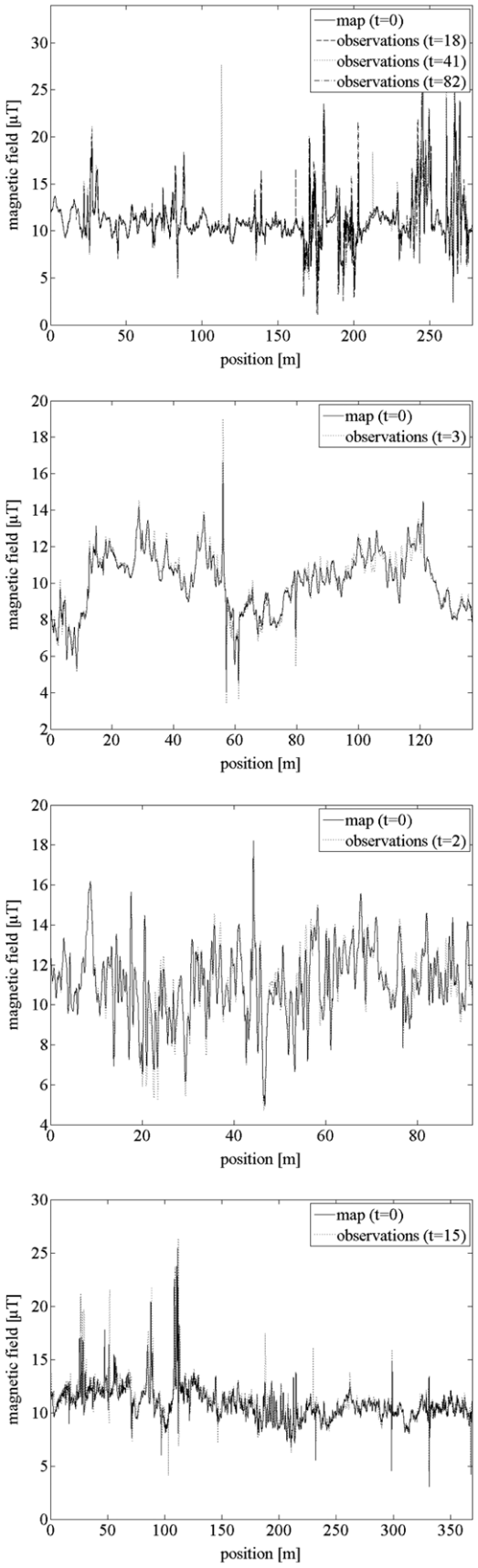

Fig. 5. The magnetic field data. From top to bottom: Computer Engineering Laboratory, University Hospital of Oulu, campus library of University of Oulu, and University of Oulu campus area. Time units in legends are days. The plot shows $\|\boldsymbol{m}\|$ as a function of the position along the path.

arbitrarily close approximate fair samples from $p(x_t|z_t)$. See [21, 9,10] for a more thorough discussion of particle filters and MCL. The main steps of the particle filter are also presented as the part of Procedure 1, which shows the basic MCL algorithm applying multivariate Gaussian measurement model with mean $h(\boldsymbol{x})$ and covariance $\boldsymbol{R}$

$$p(\boldsymbol{z}|\boldsymbol{x}) = \frac{1}{(2\pi)^{N/2}\,|\boldsymbol{R}|^{1/2}} \exp\left(-\frac{1}{2}(\boldsymbol{z}-h(\boldsymbol{x}))^{\mathrm{T}}\boldsymbol{R}^{-1}(\boldsymbol{z}-h(\boldsymbol{x}))\right) \quad (1)$$

where $\boldsymbol{x} = [x \quad \theta]$ is the state vector for the one-dimensional case whose elements are position x and heading θ (either 0 or π in the one-dimensional experiments reported here), $\boldsymbol{z}$ is an observation made from the magnetic vector field $\boldsymbol{B}$, and $h : \mathbb{R}^n \longrightarrow \mathbb{R}^3$ maps each n-dimensional (here $n = 2$) state $\boldsymbol{x}$, representing the pose of the robot, to an observation $\boldsymbol{z}$ based on the map. The use of $\|\boldsymbol{m}\|$ as an observation z yields to the single variable Gaussian probability density function with mean $\|h(x)\|$ and variance σ_r^2

$$p(z|\boldsymbol{x}) = \frac{1}{\sigma_r\sqrt{2\pi}} \exp\left(-\frac{(z-\|h(\boldsymbol{x})\|)^2}{2\sigma_r^2}\right). \quad (2)$$

In Procedure 1, x_{start} represents the unknown starting position of the robot at the beginning of the experiment. This position is incremented by 1 m for each subsequent experiment in order to test the effect of the initial position of the robot on the localization performance. The performance might be affected by, *e.g.*, sensor aliasing and differences between the map and the observation data. In the experiments, the motion model of the localization target was

$$\hat{x}_t = x_{t-1} + w(\theta) \quad (3)$$

where $w(\theta) \sim \mathcal{N}(\pm 0.25\text{ m}, \sigma_q^2 = 0.001\text{ m}^2)$ for which the mean is $+0.25$ m and -0.25 m for $\theta = 0$, and $\theta = \pi$, respectively.

Procedure 1

Require: $p(\boldsymbol{z}|x) \sim \mathcal{N}(h(x), R)$
  generate $N/2$ particles with $x = [0, x_{max}]$ and $\theta = 0$
  generate $N/2$ particles with $x = [0, x_{max}]$ and $\theta = \pi$
  $\Delta x \leftarrow 0$
  $x_{correct} \leftarrow x_{start}$
  while $\Delta x \leq \Delta x_{max}$ **do**
    $x_{correct} \leftarrow x_{correct} + w(0)$
    $\boldsymbol{z}_t \leftarrow h_{obs}(x_{correct})$
    $\Delta x \leftarrow x_{correct} - x_{start}$
    for all N particles **do**
      $\hat{x}_t^{(n)} \leftarrow x_{t-1}^{(n)} + w(\theta^{(n)})$
      $\pi_t^{(n)} \leftarrow \pi_{t-1}^{(n)} p(\boldsymbol{z}_t|\hat{x}_t^{(n)})$
    end for
    if $\frac{1}{\sum_{n=1}^{N}(\pi^{(n)})^2} < N/2$ **then**
      draw N samples from $\tilde{p}(\boldsymbol{x}_t|\boldsymbol{z}_t)$
      $\pi^{(n)}$ are normalized to sum 1
      $\hat{x} \leftarrow \sum_{n=0}^{N} \pi^{(n)} x^{(n)}$
      $e \leftarrow |\hat{x} - x_{correct}|$
      for all N particles **do**
        $\pi^{(n)} \leftarrow 1$
      end for
    end if
  end while

The observation for the correct state $\boldsymbol{x}_{\text{correct}}$ was obtained from the observation data (instead of map data). Function $h_{obs}(\boldsymbol{x})$ was used to map $\boldsymbol{x}$ to an observation $\boldsymbol{z}$ from the magnetic vector field $\boldsymbol{B}$. The maximum distance $\Delta x_{\max}$ the robot was allowed to travel was predefined. In the reported experiments $\Delta x_{\max} = 100$ m was used, *i.e.*, the localization target was allowed to travel 100 m (maximum) from the starting position x_{start}. Consequently, the

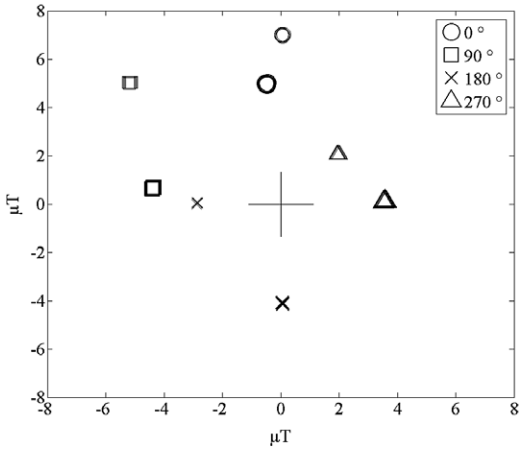

Fig. 6. The effect of calibration. Grey symbols represent uncorrected measurements and black symbols the measurements corrected using the transformation $\boldsymbol{A}$ found by the calibration procedure.

position of the target had to be estimated during that travel. If the estimation error e was $\geq$ 2.0 m for robot, and e $\geq$ 5.0 m for person localization experiments after the completion of the experiment, the experiment was considered failed. In Procedure 1 effective sample size criterion [22] was used for resampling, *i.e.*, resampling was performed *iff*

$$\frac{1}{\sum_{n=1}^{N}(\pi^{(n)})^2} < N/2. \tag{4}$$

Between resamplings, particle weights were updated in the multiplicative manner as shown in Procedure 1. In the resampling step a new set of $N = 4000$ particles was drawn from the *posterior* $\tilde{p}(\boldsymbol{x_t}|\boldsymbol{z}_t)$ with the probability $\pi^{(n)}$, where n represents the index of the particle. At the beginning of experiments particles were divided into two sets of equal size (2000/2000), both sets assumed different direction of travel, *i.e.*, the direction of travel of the localization target along the path was assumed to be unknown (0° or 180°). The Matlab implementation of the localization algorithm, presented in Procedure 1, was capable of running (well above) in real-time with particle counts $\leq$ 4000 on a standard desktop computer.

3. Calibration

Proper calibration of the measurement system is required in order to compensate the effects of possible sensor inclination errors with regard to the world coordinate system (floor plane). These errors may arise due to tilt of the robot or 3-axis magnetometer, or non-orthogonal sensor axes. If possible inclination errors are not compensated, an observation $\boldsymbol{m}$ from the magnetic vector field B does not transform correctly, with regard to the world coordinate system, under a robot (sensor) rotation, which is illustrated in Fig. 6. Grey symbols in Fig. 6 represent observations made from the magnetic field (projected to xy-plane) before applying a calibration transform, and black symbols represent the same observations after the transform has been applied in order to compensate the inclination errors of the measurement system. All measurements in Fig. 6 were made at the same xy location of the sensor at four different angles (around z-axis). Fig. 6 illustrates how the calibration makes the observations to transform correctly under the sensor (robot) rotation, which is required for the proper operation of mapping $h : \boldsymbol{x} \longrightarrow h(\boldsymbol{x})$ (the same applies to h_{obs}).

Two data sets were collected for the calibration procedure. For the first data set the robot was manually driven along a straight line (≈9 m) while the magnetometer readings were stored. The second data set was collected by driving the robot along the same path but in reverse direction after which the set was re-indexed (mirrored) in order to align the two data sets. This procedure provided two arbitrary data sets for two different heading (0 and π) of the sensor. In an ideal (error free) case these two data sets should look similar after rotating each magnetometer reading $\boldsymbol{m}$ in one of the sets by π around z-axis. If sensor inclination errors exist, a transform $\boldsymbol{A}$ is needed, which maps sensor readings into a same coordinate system where they transform correctly under a robot (sensor) rotation around z-axis, *i.e.*, having the two calibration data sets a transform A needs to be found with property

$$m_2 = \boldsymbol{A}^{-1}\boldsymbol{\Theta}_{\pi_z}\boldsymbol{A}\boldsymbol{m}_1 \tag{5}$$

where A is an unknown 3 × 3 transformation matrix (affine transformation without translation component), $\boldsymbol{\Theta}_{\pi_z}$ is the known rotation matrix (180° around z-axis), m_1 is a measurement in the first data set, and m_2 is the corresponding measurement in the second data set, *i.e.*, m_2 has been measured in the same position with m_1 along the path but using the different sensor heading.

Finding the transformation A is a nonlinear parameter estimation problem, which can be solved, *e.g.*, by applying Levenberg–Marquardt algorithm [23]. Even though the calibration data was collected only for two different headings (0° and 180°), the transformation A will apply correctly to all possible sensor orientations around z-axis.

4. Results

Fig. 7 shows an example of a one-dimensional global self-localization experiment conducted in the Computer Engineering Laboratory. The robot starts from an unknown position (x_{start} = 140 m) and drives toward $x_{\max} = 278$. After traveling approximately 10 m the true position (shown with ○) has been correctly estimated (shown with ×).

Table 1 summarizes the global self-localization experiments where $\|\boldsymbol{m}\|$ was used as the observation z from $\boldsymbol{B}$. Each table row represents one set of experiments where each individual experiments had a different starting position: this position was incremented by 1 m for each experiment of the set. For example, an experiment set conducted in Computer Engineering Laboratory (CL) consists of 278 individual experiments (path length was 278 m). In data column of Table 1 the following symbols have been used: CL (Computer Engineering Laboratory), HP (University Hospital of Oulu), LB (Campus Library), CA (University Campus), and PR (Person self-localization). All person self-localization experiments were conducted in Computer Engineering Laboratory. Letter D following a number indicates how many days after the creation of the map the observation data used in the experiment set was acquired (e.g. CL/D41). In Table 1 symbols $\hat{e}$, σ_e, $\hat{d}$, σ_d, and f_r are used for mean estimation error, std. of estimation error, mean localization distance, std. of localization distance, and the failure rate in per cent, correspondingly.

Each experiment set was conducted using different values of the standard deviation of the measurement model σ_r from range [1.0 μT, 5.0 μT]. Increasing σ_r increases the average distance $\hat{d}$ the robot needs to travel to get localized. Larger values of σ_r make the algorithm less sensitive to local variations of the map, which increases the variance of *posterior* distribution $\tilde{p}(\boldsymbol{x_t}|\boldsymbol{z_t})$ and makes the algorithm converge more slowly. On the other hand, smaller values of σ_r make the algorithm more sensitive to noise and differences between the map and the observation data, which may cause localization to fail. Fig. 8 illustrates the relationship between σ_r and $\hat{d}$, which is nearly linear.

Table 1 also shows that person self-localization, without proper odometric information, suffers from large bias in position

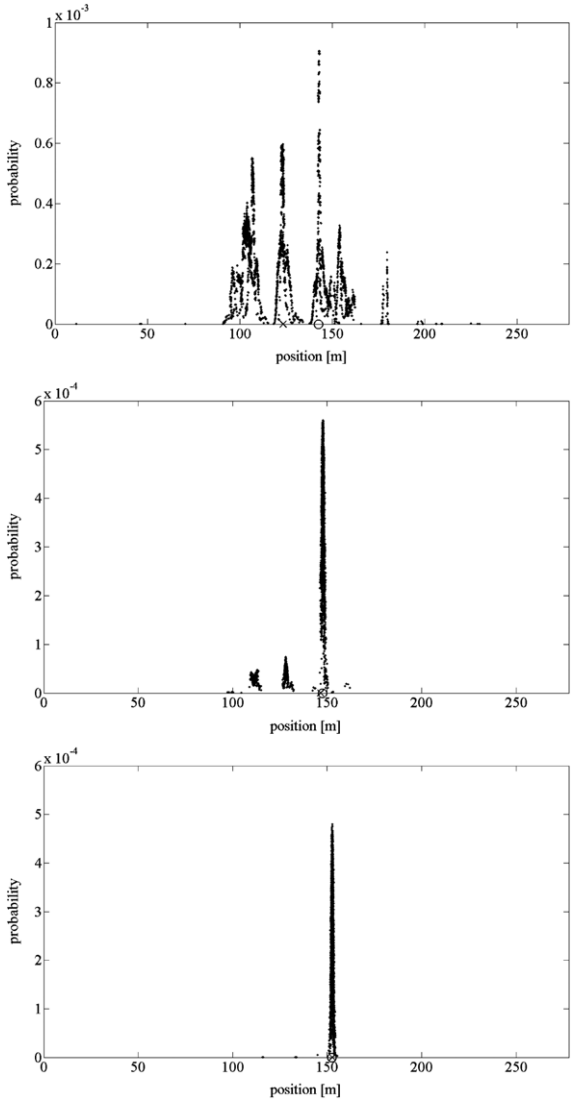

Fig. 7. A global self-localization experiment where the robot starts from position $x_{\text{start}} = 140$ m. The three figures illustrate how the particles concentrate near true position after the robot has traveled approximately 10 m. This individual belongs to experiment set CL/D82 ($\sigma_R = 3.0$) in Table 2.

estimates, *i.e.*, $\hat{e}$ is significantly larger than in robot localization experiments. This is due to discrepancies between map and observation data as can been observed from Fig. 11, which shows the magnetic field data collected for person self-localization experiments.

Table 2 shows the results of the global self-localization experiments where three-dimensional vector $\boldsymbol{m}$ was directly used as the observation $\boldsymbol{z}$ from $\boldsymbol{B}$. Each experiment set was conducted using different values of the standard deviation σ_R of the measurement model from range [1.0 μT, 3.0 μT]. Correspondingly σ_R^2 represents the identical values of diagonal elements of the covariance matrix $\boldsymbol{R}$ in Eq. (1).

Table 2 clearly illustrates the benefits of using all available information provided by the magnetic vector field. Excluding the person localization, the mean localization distance $\hat{d}$ and its std. σ_d are significantly smaller compared to results in Table 1. However, the results of person localization experiments in Table 2 shows an important exception, *i.e.*, when sensor placement is not controlled and no proper information about the angular and linear motion of the sensor is available the localization algorithm fails in cases where vector $\boldsymbol{m}$ is used as an observation. On the other hand, by using the rotation invariant observation $\|\boldsymbol{m}\|$ it is still possible to achieve relatively good localization performance, as is shown in Table 1. By utilizing inertial sensors it is possible to estimate the motion of the sensor system in a person self-localization system and to utilize $\boldsymbol{m}$ as the observation for enhanced localization performance. This issue however will be addressed elsewhere.

Table 1
Results of experiments using $\|\boldsymbol{m}\|$ as the observation.

Data	σ_r (μT)	$\hat{e}$ (m)	σ_e (m)	$\hat{d}$ (m)	σ_d (m)	f_r (%)
CL/D41	1.0	0.13	0.16	6.00	7.91	7.2
CL/D41	3.0	0.10	0.07	11.34	6.26	1.1
CL/D41	5.0	0.10	0.07	21.73	12.41	0
CL/D82	1.0	0.12	0.09	5.94	5.45	3.2
CL/D82	3.0	0.12	0.06	12.51	6.09	0
CL/D82	5.0	0.12	0.07	21.60	11.63	0
HP/D03	1.0	0.31	0.08	5.79	3.25	0.7
HP/D03	3.0	0.28	0.05	14.56	4.68	0
HP/D03	5.0	0.28	0.04	21.01	6.62	0
LB/D02	1.0	0.31	0.07	2.96	1.31	0
LB/D02	3.0	0.30	0.04	5.90	1.75	0
LB/D02	5.0	0.29	0.03	10.88	3.65	0
CA/D15	1.0	0.63	0.23	10.76	9.93	10.3
CA/D15	3.0	0.71	0.29	19.55	8.62	0
CA/D15	5.0	0.72	0.18	31.59	14.97	1.4
PR/D05	1.0	3.47	1.87	9.98	4.02	2.9
PR/D05	3.0	3.46	1.86	23.98	7.57	0
PR/D05	5.0	3.43	2.04	45.02	12.04	0.4

Table 2
Results of experiments using $\boldsymbol{m}$ as the observation.

Data	σ_R (μT)	$\hat{e}$ (m)	σ_e (m)	$\hat{d}$ (m)	σ_d (m)	f_r (%)
CL/D41	1.0	0.11	0.08	1.28	0.87	2.5
CL/D41	2.0	0.10	0.08	2.20	1.48	0
CL/D41	3.0	0.10	0.08	3.26	2.24	0
CL/D82	1.0	0.12	0.07	1.28	0.91	1.4
CL/D82	2.0	0.12	0.07	2.23	1.52	0
CL/D82	3.0	0.11	0.07	3.30	2.16	0
HP/D03	1.0	0.29	0.07	0.74	0.54	0
HP/D03	2.0	0.29	0.05	1.37	1.02	0
HP/D03	3.0	0.28	0.05	2.25	1.70	0
LB/D02	1.0	0.28	0.05	0.50	0.30	0
LB/D02	2.0	0.28	0.05	0.82	0.54	0
LB/D02	3.0	0.28	0.05	1.63	0.71	0
CA/D15	1.0	0.71	0.30	1.69	1.65	3.0
CA/D15	2.0	0.71	0.31	2.78	1.94	0.5
CA/D15	3.0	0.71	0.29	4.12	2.07	0
PR/D05	1.0	1.51	1.00	34.56	1.91	97.8
PR/D05	2.0	3.35	1.31	33.13	5.51	92.1
PR/D05	3.0	3.55	1.05	22.52	12.32	81.3
PR/D05	4.0	2.90	1.44	20.17	10.74	57.6

For the discussion about the stability of the magnetic field the standard deviation of $\|\boldsymbol{m}\|$ (in CL) as a function of x is presented in Fig. 9. Five data sets between $t = [0, 81]$ (days) were used to compute the standard deviation. Part of deviations can be explained by the odometric noise. The high values of standard deviation can be however associated to local peaks of the magnetic field. These peaks exist near doors connecting two corridors (the doors have a steel frame), or near elevators as it is the case for $x \approx 245$ m (elevator 1 in Fig. 3), and $x \approx 265$ m (elevator 2 in Fig. 3). Variances of the magnetic field introduced by the elevators and the doors are mainly caused by deviations in the measurement path in y direction when the robot is driven manually along the measurement path. Near large gradients of the magnetic field deviations from the center line of the corridor cause larger deviations to magnetic field measurements compared to areas where the magnetic field is more

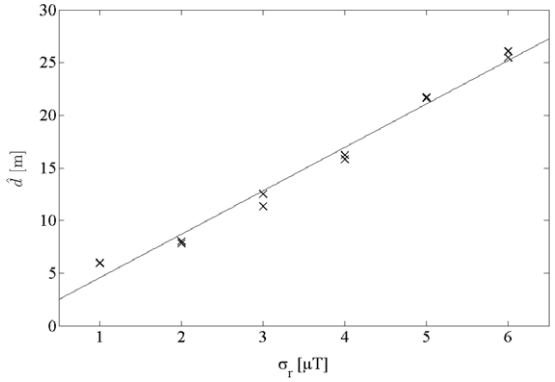

Fig. 8. The average distance $\hat{d}$ the robot needs to travel in order to get localized as a function of σ_r. This data is from the experiments CL/D41 and CL/D82 (see Table 1).

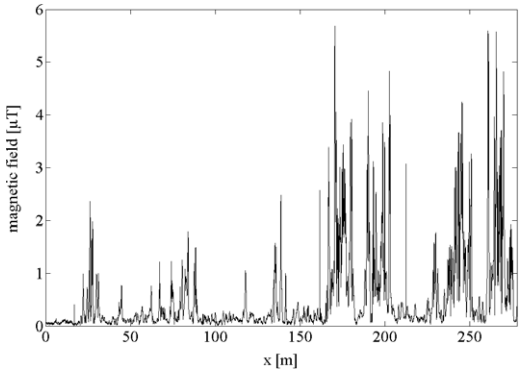

Fig. 9. The standard deviation of the magnetic field as a function of the robot position x along the measurement path (CL).

uniform. An example of a strong magnetic field can bee seen in Fig. 10, which shows the two-dimensional map of the magnetic field of the first 70 m of the measurement path (CL). The magnetic field around $x \approx 22$ m is caused by the door 1 shown in Fig. 3. A small deviations in the position of the robot in y direction near $x \approx 22$ m can cause relatively large deviations in magnetic field measurements, which explains the higher variance around $x \approx 22$ m in Fig. 9. Fig. 10 illustrates how the magnetic field inside the building varies (at least) in two dimensions, which is the necessary prerequisite for applying the presented approach to *two-dimensional* self-localization problems. The magnetic map shown in Fig. 10 was created by measuring the magnetic field along multiple longitudinal, parallel paths and by interpolating the measurements to provide the two-dimensional map.

5. Conclusion

Localization is one of the fundamental problems in mobile robotics, as in many applications a robot needs to know its location in order to perform its tasks. In this article, a global self-localization technique that utilizes observations of the ambient magnetic field was proposed. This study was inspired by the evidence that animals use the magnetic field of Earth for true navigation. The experiments reported in this article suggest that (especially) modern buildings with reinforced concrete and steel structures have unique, spatially varying ambient magnetic fields that can be used for navigation in very much the same way as Earth's magnetic field, but on a smaller scale. In principle, a non-uniform ambient magnetic field produces different observations, depending on the path taken through it. The reported experiments demonstrate the feasibility of the proposed approach. The approach provides a

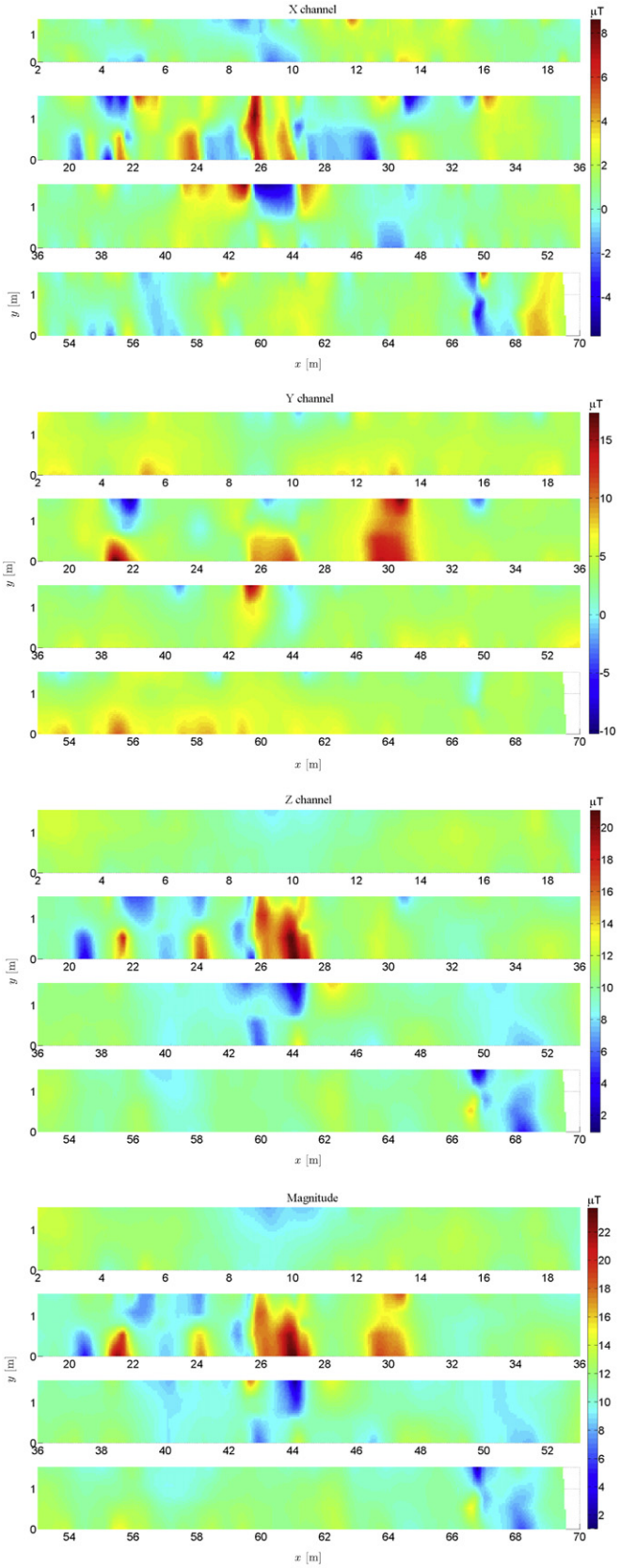

Fig. 10. The magnetic field of a corridor in Computer Engineering Laboratory. A two-dimensional map of the magnetic field of the first 70 m of the measurement path (CL). From top to bottom: m_x, m_y, m_z, and $\|\boldsymbol{m}\|$ as a function of xy position.

promising and simple alternative for solving the global indoor self-localization problem. The presented technique was applicable for

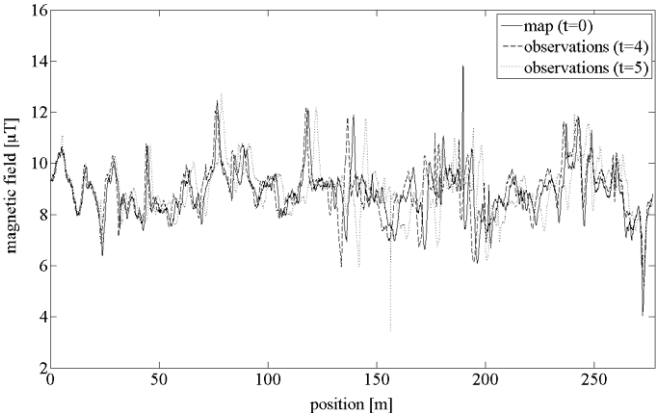

Fig. 11. The magnetic field data collected for the person self-localization experiments.

a one-dimensional localization problem, *i.e.*, for localizing a robot or a person within corridors. However, the proposed approach can be generalized to two- or three-dimensional localization problems, assuming that maps can be provided. In some applications the proposed approach may provide an alternative to machine vision [24–26] based approaches, especially when only one-dimensional localization is needed or when the illumination of the environment changes. On the other hand, the proposed technique may also be used in parallel with machine vision and range finder based approaches in order to overcome possible sensor aliasing problems.

The reported experiments suggest that the ambient magnetic field may remain sufficiently stable for longer periods of time. In the reported experiments the magnetic field remained nearly unchanged, although some variations were observed. These variations did not have a large impact on the localization performance, however. On the other hand, the magnetic field is not sensitive to many environmental changes that may affect other localization techniques such as vision or range finder based techniques, which rely on visual or geometrical features. For example, the magnetic field is not sensitive to non-magnetic dynamic or static objects or changes in illumination.

References

[1] Larry C. Boles, Kenneth J. Lohmann, True navigation and magnetic maps in spiny lobsters, Nature 421 (2003) 60–63.
[2] W. Wiltschko, R. Wiltschko, Magnetic compass of european robins, Science 176 (1972) 62–64.
[3] T.H. Maugh, Magnetic navigation an attractive possibility, Science 215 (1982) 1492–1493.
[4] H. Mouritsen, G. Feenders, M. Liedvogel, W. Kropp, Migratory birds use head scans to detect the direction of the earths magnetic field, Current Biology 9 (2004) 1946–1949.
[5] C.V. Mora, M. Davison, J.M. Wild, M.M. Walker, Magnetoreception and its trigeminal mediation in the homing pigeon, Nature 432 (2004) 508–511.
[6] M. Kisliuk, J. Ishay, Influence of an additional magnetic field on hornet nest architecture, Cellular and Molecular Life Sciences (CMLS) 33 (1977) 885–887.
[7] J.L. Kirschvink, D.S. Jones, B.J. MacFadden, Magnetite Biomineralization and Magnetoreception in Organisms: A New Biomagnetism, Springer, 1985.
[8] Joseph L. Kirschvink, Michael M. Walker, Carol E. Diebel, Magnetite-based magnetoreception, Current Opinion in Neurobiology 11 (2001) 462–467.
[9] F. Dellaert, D. Fox, W. Burgard, S. Thrun, Monte carlo localization for mobile robots, in: International Conference on Robotics and Automation, vol. 2, 1999, pp. 1322–1328.
[10] S. Thrun, W. Burgard, D. Fox, Probabilistic Robotics, MIT Press, 2005.
[11] John Burnett, Patrick Du Yaping, Mitigation of extremely low frequency magnetic fields from electrical installations in high-rise buildings, Building and Environment 37 (2002) 769–775.
[12] International Agency for Research on Cancer, Non-ionizing radiation, part 1: Static and extremely low-frequency (elf) electric and magnetic fields, in: IARC Monographs on the Evaluation of Carcinogenic Risks to Humans, World Health Organization, 2002.
[13] K. Yamazaki, K. Kato, K. Ono, H. Saegusa, K. Tokunaga, Y. Iida, S. Yamamoto, K. Ashiho, K. Fujiwara, N. Takahashi, Analysis of magnetic disturbance due to buildings, IEEE Transactions on Magnetics 39 (2003) 3226–3228.
[14] G. Casinovi, A. Geri, G.M. Veca, Magnetic field near a concrete wall during a lightning stroke, IEEE Transactions on Magnetics 25 (1989) 4006–4008.
[15] Hao Lu, Jiyin Zhao, Xiaomeng Li, Jianpo Li, A new method of double electric compass for localization, in: Proceedings of the 6th World Congress on Intelligent Control and Automation, 2007.
[16] S. Suksakulchai, S. Thongchai, D.M. Wilkes, K. Kawamura, Mobile robot localization using an electronic compass for corridor environment, in: 2000 IEEE International Conference on Systems, Man, and Cybernetics, 2000.
[17] I. Nygren, M. Jansson, Terrain navigation for underwater vehicles using the correlator method, IEEE Journal of Oceanic Engineering 29 (2004) 906–915.
[18] C. Tyren, Magnetic terrain navigation, in: Proceedings of the 1987 5th International Symposium on Unmanned Untethered Submersible Technology, vol. 5, 1987, pp. 245–256.
[19] R. Karlsson, F. Gustafsson, Particle filter for underwater terrain navigation, in: IEEE Workshop on Statistical Signal Processing, 2003.
[20] B.D. Ripley, Stochastic Simulation, Wiley, New York, 1987.
[21] S. Arulampalam, S. Maskell, N. Gordon, T. Clapp, A tutorial on particle filters for on-line non-linear/non-gaussian bayesian tracking, IEEE Transactions on Signal Processing 50 (2) (2002) 174–188.
[22] A. Doucet, N. de Freitas, N. Gordan, Sequential Monte Carlo Methods in Practice, Springer-Verlag, 2001.
[23] Donald Marquardt, An algorithm for least-squares estimation of nonlinear parameters, SIAM Journal on Applied Mathematics 11 (1963) 431–441.
[24] E. Menegatti, A. Pretto, A. Scarpa, E. Pagello, Omnidirectional vision scan matching for robot localization in dynamic environments, IEEE Transactions on Robotics 22 (2006) 523–535.
[25] J. Wolf, W. Burgard, H. Burkhardt, Robust vision-based localization by combining an image-retrieval system with monte carlo localization, IEEE Transactions on Robotics 21 (2005) 208–216.
[26] F. Dellaert, W. Burgard, D. Fox, S. Thrun, Using the condensation algorithm for robust, vision-based mobile robot localization, in: IEEE Computer Society Conference on Computer Vision and Pattern Recognition, 1999.

Janne Haverinen obtained his Diploma degree and Ph.D. in computer engineering from the University of Oulu, Finland in 1996, and 2004, respectively. At present he is an acting professor in the Intelligent Systems Group in the Department of Electrical and Information Engineering of University of Oulu. His current research focuses on multirobot systems, evolutionary robotics, and robot localization.

Anssi Kemppainen obtained his Diploma degree in computer engineering from the University of Oulu, Finland in 2005. At present he is a researcher in the Intelligent Systems Group in the Department of Electrical and Information Engineering of University of Oulu. His current research focuses on multirobot systems and optimal spatial sampling.